Journal of Advanced Research 8 (2017) 655–661

Contents lists available at ScienceDirect

Journal of Advanced Research

journal homepage: www.elsevier.com/locate/jare

Original Article

Convective thermal and concentration transfer effects in hydromagnetic peristaltic transport with Ohmic heating

F.M. Abbasi [a], S.A. Shehzad [b,*]

[a] Department of Mathematics, COMSATS Institute of Information Technology, Islamabad 44000, Pakistan
[b] Department of Mathematics, COMSATS Institute of Information Technology, Sahiwal, Pakistan

GRAPHICAL ABSTRACT

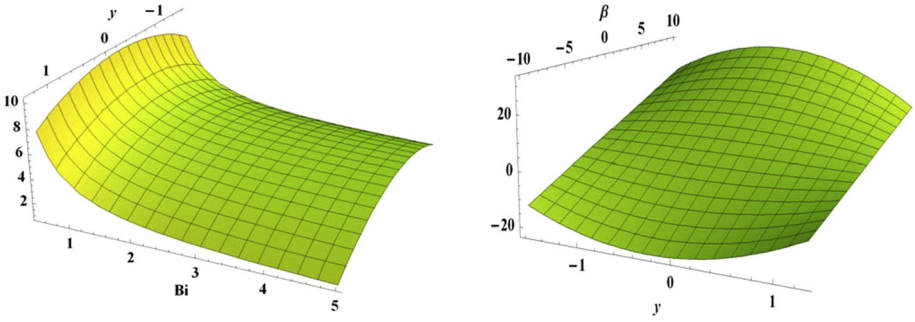

ARTICLE INFO

Article history:
Received 8 April 2017
Revised 3 August 2017
Accepted 5 August 2017
Available online 19 August 2017

Keywords:
Peristaltic transport
Soret-Dufour phenomenon
Ohmic heating
Convective conditions

ABSTRACT

The primary theme of this communication is to employ convective condition of mass transfer in the theory of peristalsis. The magnetohydrodynamic (MHD) peristaltic transport of viscous liquid in an asymmetric channel was considered for this purpose. Effects of Ohmic heating and Soret and Dufour are presented. The governing mathematical model was expressed in terms of closed form solution expressions. Attention has been focused to the analysis of temperature and concentration distributions. The graphical results are presented to visualize the impact of sundry quantities on temperature and concentration. It is visualized that the liquid temperature was enhanced with the enhancing values of Soret-Dufour parameters. The liquid temperature was reduced when the values of Biot number were larger. It is also examined that mass transfer Biot number for one wall has no impact on transfer rate. Different mass transfer Biot numbers generate a non-uniform concentration profile throughout the channel cross section.

Introduction

It is well established fact that "peristalsis" is a mechanism of liquid transport produced by progressive wave of area expansion or contraction in length of a distensible tube containing fluid. At present, the physiologists considered it one of key mechanisms of liquid transport in various biological processes. Especially, it occurs in ovum movement of female fallopian tube, urine transport in the ureter, small blood vessels vasomotion, food swallowing via esophagus and many others. Mechanism of peristalsis has important applications in many appliances of modern biomedical engineering include heart-lung machine, dialysis machines and blood pumps. Apart from physiology and biomedical engineering, this type of mechanism is utilized in many engineering devices where

Peer review under responsibility of Cairo University.
* Corresponding author.
E-mail address: ali_qau70@yahoo.com (S.A. Shehzad).

http://dx.doi.org/10.1016/j.jare.2017.08.003
2090-1232/

the fluid is meant to be kept away from direct contact of machinery. Modern pumps are also designed through principle of peristalsis. Initial seminal works on the peristaltic motion was addressed by Latham [1] and Shapiro et al. [2]. Available literature on peristalsis through various aspects is quite extensive. Interested readers may be directed to some recent investigations on this topic [3–15].

Analysis of temperature and mass species transport is important for better understanding of any physical system. This is because of the fact that temperature and mass species transfer are not only vital in energy distribution of a system but also they greatly influence the mechanics of the systems. Clearly the relations between their driving potentials are more complicated when temperature and concentration phenomenon is occurred simultaneously in a system. Energy flux produced by concentration gradients is called Dufour effect while mass flux induced by energy gradient is known as Soret effect. No doubt, there is key importance of heat and mass transport in exchange of gases in lungs, blood purification in kidney, maintaining body temperature of warm blooded species, perspiration in hot weather, water and food transport from roots to all parts of plants, metal purification, controlled nuclear reaction etc. Also Soret-Dufour phenomenon has major importance in mixture of gases having medium and lighter molecular weights and in isotope separation. However, it is observed that almost all the previous contributions on peristalsis with heat transfer are presented via prescribed surface temperature or heat flux. The published studies about peristaltic flows subject to convective conditions of temperature are still scarce. From literature review, we stand out the following works by Hayat et al. [16] and Abbasi et al. [17].

Although peristaltic motion through heat and mass transport phenomenon is discussed but no information is yet available about peristaltic motion subject to convective condition for concentration. The aim here is to utilize such condition in the peristaltic flows. Therefore, the present attempt examines the MHD peristaltic flow of viscous fluid in an asymmetric channel with Joule heating and convective conditions for temperature and concentration distributions. Lubrication approach is used in the performed analysis. Temperature and concentration distributions are analyzed for various embedded parameters in the problem formulation. It is expected that presented analysis will provide a basis for several future investigations on the topic.

Mathematical formulation

We consider the peristaltic flow in an asymmetric channel with width $d_1 + d_2$. The considered liquid is electrically conducting through applied magnetic field B_0. A uniform magnetic field is applied in the $\overline{Y}-$ direction (see Fig. 1). An incompressible liquid is taken in channel. The flow is induced due to travelling waves along the channel walls. The wave shapes can be taken into the forms give below:

$$\overline{H}_1(\overline{X},\bar{t}) = \varepsilon_1 + d_1, \textit{Upperwall}; \overline{H}_2(\overline{X},\bar{t}) = -(\varepsilon_2 + d_2), \textit{Lowerwall}.$$

Here the disturbances generated due to propagation of peristaltic waves at the upper and lower walls are denoted by ε_1 and ε_2, respectively. The values of ε_1 and ε_2 are defined by

$$\varepsilon_1 = a\cos\left(\tfrac{2\pi}{\lambda}(\overline{X} - c\bar{t})\right),$$
$$\varepsilon_2 = b\cos\left(\tfrac{2\pi}{\lambda}(\overline{X} - c\bar{t}) + \alpha\right),$$

here a, b represent the amplitudes of waves, λ the wavelength and α the phase difference of waves. A schematic diagram of such an asymmetric channel has been provided through Fig.1a. The low magnetic Reynolds number assumption leads to ignorance of induced magnetic field. The upper and lower walls satisfy the convective conditions through temperature and concentration distributions. The basic laws which can govern the present flow analysis are

$$\overline{\nabla}.\overline{V} = 0,$$

$$\rho\frac{d\overline{V}}{dt} = -\overline{\nabla P} + \mu(\nabla^2\overline{V}) + \overline{J}\times\overline{B}.$$

In above equations $\overline{V} = [U(\overline{X},\overline{Y},\bar{t}), V(\overline{X},\overline{Y},\bar{t}), 0]$ is the velocity field, $\overline{P}$ is the pressure, μ is the dynamic viscosity, $\frac{d}{dt}$ is the material time derivative, $\bar{t}$ is the time, ρ is the fluid density, $\overline{J}$ is the current density and $\overline{B}$ is the applied magnetic field. Using the assigned values of velocity field, we have the following expressions:

$$\overline{U}_{\overline{X}} + \overline{V}_{\overline{Y}} = 0, \tag{1}$$

$$\overline{U}_{\bar{t}} + \overline{V}\overline{U}_{\overline{Y}} + \overline{U}\overline{U}_{\overline{X}} = -\frac{1}{\rho}\overline{P}_{\overline{X}} + \upsilon(\overline{U}_{\overline{X}\overline{X}} + \overline{U}_{\overline{Y}\overline{Y}}) - \frac{\sigma}{\rho}B_0^2\overline{U}, \tag{2}$$

$$\overline{V}_{\bar{t}} + \overline{V}\overline{V}_{\overline{Y}} + \overline{U}\overline{V}_{\overline{X}} = -\frac{1}{\rho}\overline{P}_{\overline{Y}} + \boldsymbol{\upsilon}\left[\overline{V}_{\overline{X}\overline{X}} + \overline{V}_{\overline{Y}\overline{Y}}\right], \tag{3}$$

The energy and concentration equations are

$$C_p(T_t + \overline{U}T_{\overline{X}} + \overline{V}T_{\overline{Y}}) = \tfrac{K}{\rho}[T_{\overline{X}\overline{X}} + T_{\overline{Y}\overline{Y}}] + \upsilon\left[2(\overline{U}_{\overline{X}}^2 + \overline{V}_{\overline{Y}}^2) + (\overline{U}_{\overline{Y}} + \overline{V}_{\overline{X}})^2\right] + \tfrac{DK_T}{\rho C_s}[C_{\overline{X}\overline{X}} + C_{\overline{Y}\overline{Y}}] + \tfrac{\sigma}{\rho}B_0^2\overline{U}^2 + \tfrac{\Phi}{\rho}, \tag{4}$$

$$C_{\bar{t}} + \overline{U}C_{\overline{X}} + \overline{V}C_{\overline{Y}} = D[C_{\overline{X}\overline{X}} + C_{\overline{Y}\overline{Y}}] + \frac{DK_T}{T_m}[T_{\overline{X}\overline{X}} + T_{\overline{Y}\overline{Y}}], \tag{5}$$

where C_p the specific heat, T the temperature, $\boldsymbol{\upsilon}$ the kinematic viscosity, K the thermal conductivity, D the mass diffusivity, K_T the thermal diffusion ratio, C_s the concentration susceptibility, σ the electric conductivity, Φ the constant heat addition/absorption, C the concentration, T_m the fluid mean temperature, T_0, T_1, C_0, C_1 the temperature and concentration at the lower and upper walls respectively, and subscripts ($\overline{X}$, $\overline{Y}$, $\bar{t}$) are used for the partial derivatives.

The present phenomenon can be transfer from laboratory frame to wave frame via the following relations

$$\overline{x} = \overline{X} - c\bar{t},\ \overline{y} = \overline{Y},\ \overline{u} = \overline{U} - c,\ \overline{v} = \overline{V},\ \overline{p}(\overline{x},\overline{y}) = \overline{P}(\overline{X},\overline{Y},\bar{t}), \tag{6}$$

where 'c' is the speed of propagation of wave. Implementation of above transformations gives the following expressions

$$\frac{\partial\overline{u}}{\partial\overline{x}} + \frac{\partial\overline{v}}{\partial\overline{y}} = 0, \tag{7}$$

$$\rho\left((\overline{u}+c)\frac{\partial}{\partial\overline{x}} + \overline{v}\frac{\partial}{\partial\overline{y}}\right)(\overline{u}+c) = -\frac{\partial\overline{p}}{\partial\overline{x}} + \mu\left(\frac{\partial^2\overline{u}}{\partial\overline{x}^2} + \frac{\partial^2\overline{u}}{\partial\overline{y}^2}\right) - \sigma B_0^2(\overline{u}+c), \tag{8}$$

$$\rho\left((\overline{u}+c)\frac{\partial}{\partial\overline{x}} + \overline{v}\frac{\partial}{\partial\overline{y}}\right)\overline{v} = -\frac{\partial\overline{p}}{\partial\overline{y}} + \mu\left(\frac{\partial^2\overline{v}}{\partial\overline{x}^2} + \frac{\partial^2\overline{v}}{\partial\overline{y}^2}\right), \tag{9}$$

$$\rho C_p\left((\overline{u}+c)\tfrac{\partial}{\partial\overline{x}} + \overline{v}\tfrac{\partial}{\partial\overline{y}}\right)T = K\left(\tfrac{\partial^2 T}{\partial\overline{x}^2} + \tfrac{\partial^2 T}{\partial\overline{y}^2}\right) + \mu\left[2\{(\tfrac{\partial\overline{u}}{\partial\overline{x}})^2 + (\tfrac{\partial\overline{v}}{\partial\overline{y}})^2\} + (\tfrac{\partial\overline{v}}{\partial\overline{x}} + \tfrac{\partial\overline{u}}{\partial\overline{y}})^2\right] + \tfrac{DK_T}{C_s}\left(\tfrac{\partial^2 C}{\partial\overline{x}^2} + \tfrac{\partial^2 C}{\partial\overline{y}^2}\right) + \sigma B_0^2(\overline{u}+c) + \Phi, \tag{10}$$

$$\left((\overline{u}+c)\frac{\partial}{\partial\overline{x}} + \overline{v}\frac{\partial}{\partial\overline{y}}\right)C = D\left(\frac{\partial^2 C}{\partial\overline{x}^2} + \frac{\partial^2 C}{\partial\overline{y}^2}\right) + \frac{DK_T}{T_m}\left(\frac{\partial^2 T}{\partial\overline{x}^2} + \frac{\partial^2 T}{\partial\overline{y}^2}\right). \tag{11}$$

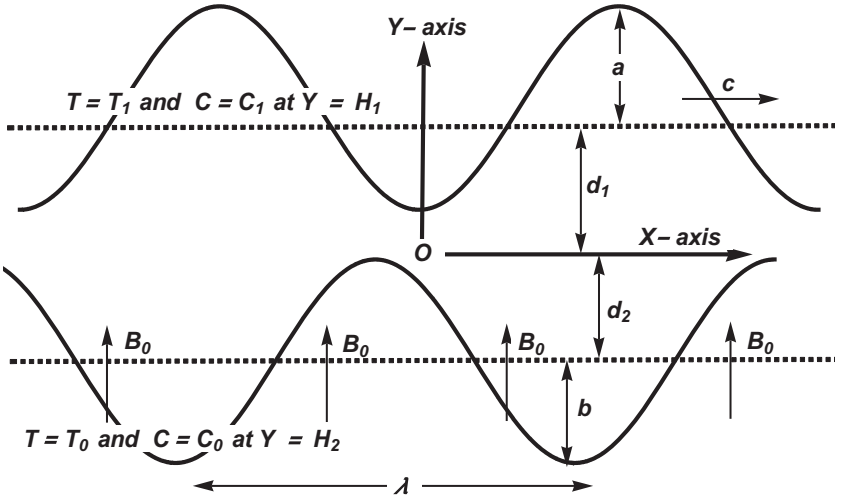

Fig. 1. Schematic picture of the asymmetric channel.

Making use of the following non-dimensional quantities

$$\begin{aligned}
&x=\tfrac{\bar{x}}{\lambda}, y=\tfrac{\bar{y}}{d_1}, u=\tfrac{\bar{u}}{c}, v=\tfrac{\bar{v}}{c\delta}, \delta=\tfrac{d_1}{\lambda}, H_1=\tfrac{\bar{H}_1}{d_1},\\
&H_2=\tfrac{\bar{H}_2}{d_1}, d=\tfrac{d_2}{d_1}, a=\tfrac{a_1}{d_1}, b=\tfrac{b_1}{d_1}, p=\tfrac{d_1^2\bar{p}}{c\lambda\mu}, \upsilon=\tfrac{\mu}{\rho},\\
&\mathrm{Re}=\tfrac{\rho c d_1}{\mu}, t=\tfrac{c\bar{t}}{\lambda}, \theta=\tfrac{T-T_0}{T_1-T_0}, \varphi=\tfrac{C-C_0}{C_1-C_0},\\
&Br=\mathrm{Pr}E, M^2=\left(\tfrac{\sigma}{\mu}\right)B_0^2a^2, E=\tfrac{c^2}{C_p(T_1-T_0)},\\
&Df=\tfrac{D(C_1-C_0)K_T}{C_sC_p\mu(T_1-T_0)}, Sr=\tfrac{\rho DK_T(T_1-T_0)}{\mu T_m(C_1-C_0)}, Sc=\tfrac{\mu}{\rho D},\\
&\beta=\tfrac{\Phi}{KT_0}, \mathrm{Pr}=\tfrac{\mu C_p}{K}, u=\psi_y, v=-\psi_x,
\end{aligned} \tag{12}$$

$$p_x=\psi_{yyy}-M^2(\psi_y+1), \tag{13}$$

$$p_y=0, \tag{14}$$

$$\theta_{yy}+Br(\psi_{yy})^2+BrM^2(\psi_y+1)^2+\mathrm{Pr}Df(\varphi_{yy})+\beta=0, \tag{15}$$

$$\frac{1}{Sc}\varphi_{yy}+Sr\theta_{yy}=0, \tag{16}$$

where *Re* is the Reynolds number, *Br* is the Brinkman number, ψ is the stream function, Pr is the Prandtl number, *E* is the Eckert number, *Sr* is the Soret number, Sc is the Schmidt number, *Df* is the Dufour number, *M* is the Hartman number, δ is the wave number, β is the dimensionless source/sink parameter, φ is dimensionless concentration and θ is the dimensionless temperature. Now expression of continuity is automatically satisfied and low Reynolds number and long wavelength approach is used in obtaining Eqs. (13)–(16).

Introducing F and η as non-dimensional mean flow rates in wave and laboratory frames, one has [15,17]:

$$\psi=\frac{e^{-My(2e^{(h_1+h_2)M}(F+h_1-h_2)-2e^{2My}(F+h_1-h_2)-e^{M(h_2+y)}(-2+FM)(h_1+h_2-2y)-e^{M(h_1+y)}(2+FM)(h_1+h_2-2y))}}{2(e^{h_1M}(e^{h_2M}(2+h_1M-h_2M)-2+h_1M-h_2M))},$$

$$\eta=F+d+1 \tag{17}$$

in which

$$F=\int_{h_2}^{h_1}\frac{\partial\psi}{\partial y}dy. \tag{18}$$

The convective temperature condition is

$$-K\frac{\partial T}{\partial Y}=l(T-T_w).$$

Here K, l and T_w represent the thermal conductivity, wall heat transfer coefficient and wall temperature, respectively. The asymmetric characteristic of channel requires considering the various coefficients of heat transfer for upper and lower walls, i.e. l_1 for upper and l_2 for lower wall. The convection condition for concentration field is

$$-D\frac{\partial C}{\partial Y}=k_m(C-C_w).$$

Here k_m the coefficient of mass transfer and C_w the concentration of wall.

The non-dimensional conditions may be imposed as follows:

$$\begin{aligned}
&\psi=\tfrac{F}{2}, \psi_y=-1, \theta_y+Bi_1\theta=0, \varphi_y+Mi_1\varphi=0, aty=h_1,\\
&\psi=-\tfrac{F}{2}, \psi_y=-1, \theta_y-Bi_2(\theta-1)=0, \varphi_y-Mi_2(\varphi-1)=0, aty=h_2,
\end{aligned} \tag{19}$$

where

$$\begin{aligned}
&h_1(x)=1+a\cos(2\pi x), h_2(x)=-d-b\cos(2\pi x+\alpha),\\
&Bi_1=\tfrac{l_1d_1}{K}, Bi_2=\tfrac{l_2d_1}{K}, Mi_1=\tfrac{k_{m1}d_1}{D}, Mi_2=\tfrac{k_{m2}d_1}{D}.
\end{aligned} \tag{20}$$

In above expressions l_1, l_2, $k_{m1}$and k_{m2} are dimensionless heat and mass transfer coefficients, $Bi_{1,2}$ are heat transfer Biot-numbers and $Mi_{1,2}$ are mass transfer Biot-numbers.

Closed form solutions of the involved systems are presented in the forms

$$\theta=\frac{1}{2A_1}(g_1-g_2)+\frac{1}{A_6}(g_3+g_4),$$

$$\varphi=\tfrac{-ScSr}{2A_1}(g_5A_{12}+e^{2h_2M}y^2g_6+e^{2h_1M}y^2g_7+2e^{(h_1+h_2)M}y^2g_8)-\tfrac{g_9}{2A_1A_{11}},$$

For the sake of simplicity, only the reduced form of the solution is presented here, where the A_is and g_is are given in Appendix. Such solutions are computed using the software Mathematica.

Graphical analysis

The primary aim of this study is to analyze the effects of convective boundary conditions in heat and mass transfer of MHD peristaltic transport through a channel. Hence the graphs of temperature and concentration curves are plotted. For this theme, the Figs. 2–4 are presented for temperature and Figs. 5 and 6 for the concentration. Fig. 2 shows an increase in temperature when Dufour and Hartman numbers are increased. Also an increase in temperature is slow for variation in Df. It is found that the temperature increases rapidly when $M > 2$, but for $M < 2$, the change in temperature for changing M is slow. Fig. 3 examines the behavior of temperature for variation in $Bi_{1,2}$.Temperature at the wall decreases with increase in the corresponding Biot number. Such variation is weak as we move away from the wall. As expected

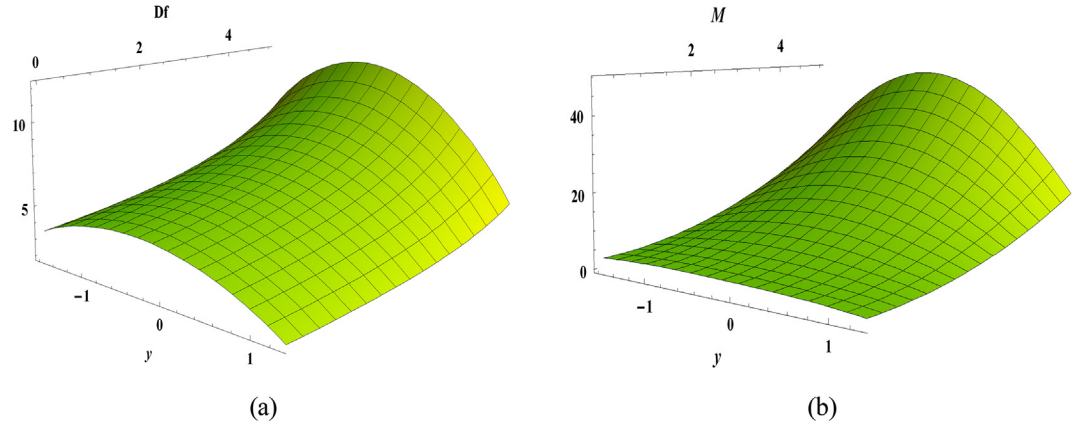

Fig. 2. Temperature variations for different Dufour and Hartman numbers when $a = 0.3$, $\beta = 0.5$, $b = 0.5$, $d = 1.2$, $Sr = 0.5$, $Br = 0.25$, $Bi_1 = 2$, $Sc = 0.5$ and $Bi_2 = 1$.

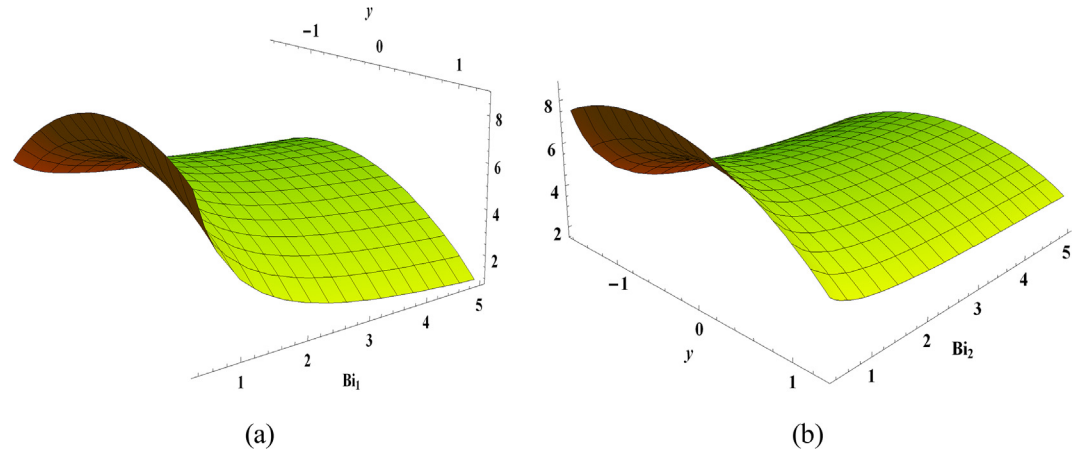

Fig. 3. Temperature variation for different heat transfer Biot-numbers when $a = 0.3$, $\beta = 0.5$, $b = 0.5$, $d = 1.2$, $Sr = 0.5$, $Br = 0.25$, $M = 1$, $Sc = 0.5$ and $Df = 1$.

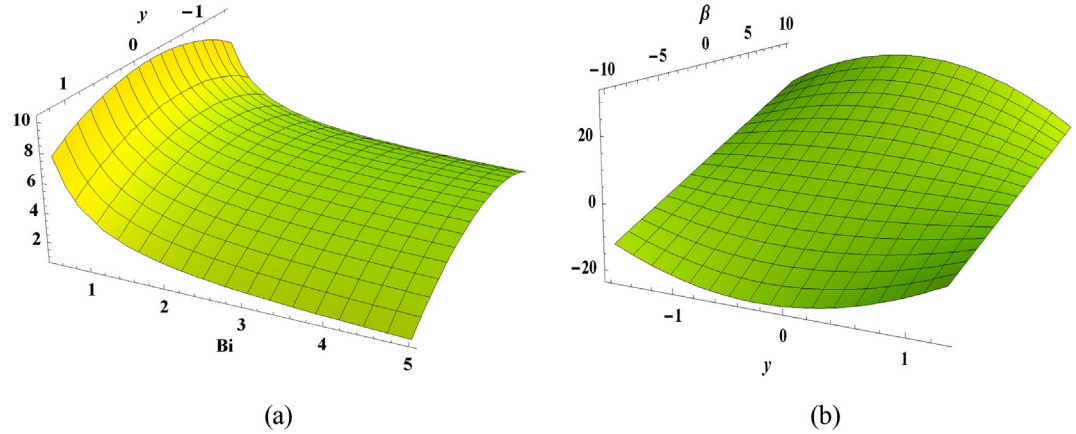

Fig. 4. Temperature variation for different heat transfer Biot-number and β when $a = 0.3$, $x = 0$, $b = 0.5$, $d = 1.2$, $Sc = 0.5$, $Br = 0.25$, $M = 1$, $Sr = 0.5$ and $Df = 1$.

the different Biot numbers for both walls generate non-uniformity in the temperature profile. This argument holds only for small values of Biot number. If the upper and lower walls have similar heat transfer coefficient then both walls have same Biot number. This situation is plotted in Fig.4(a). Here temperature decreases in view of an increase in Bi. Such decrease is more significant for $Bi \leqslant 1$. This decrease in temperature slowly vanishes when we have Biot number greater than one. Temperature increased linearly with an increase in β which corresponds to the absorption and generation of heat (as β varies from negative to positive). Negative values of variations in β indicate the presence of a heat sink within the system.

Concentration profile is examined in the Figs. 5-7. The negative value of concentration in these plots is mainly due to the concentration difference at the walls and the Soret and Dufour effects. The numbers Df and M tend to decrease the dimensionless concentration. Such decrease in concentration is slow for $Df \leqslant 2.5$ beyond which the variation in concentration becomes more significant

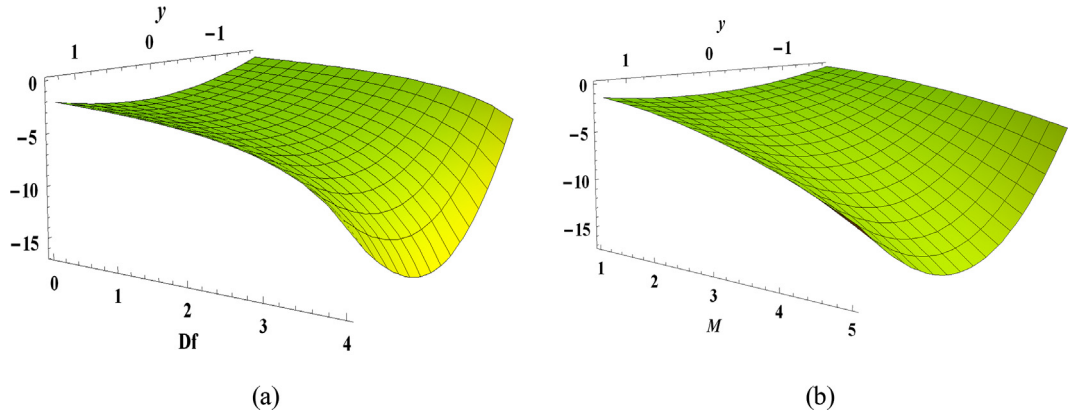

Fig. 5. Concentration variation for different Dufour and Hartman numbers when $a = 0.3$, $x = 0$, $b = 0.5$, $d = 1.2$, $Sc = 0.7$, $\eta = 1.6$, $Bi_1 = 2$, $Bi_2 = 1$, $Mi_1 = 1$, $Mi_2 = 2$, $Sr = 0.5$, $Br = 0.16$, $Sr = 0.7$ and $\beta = 1$.

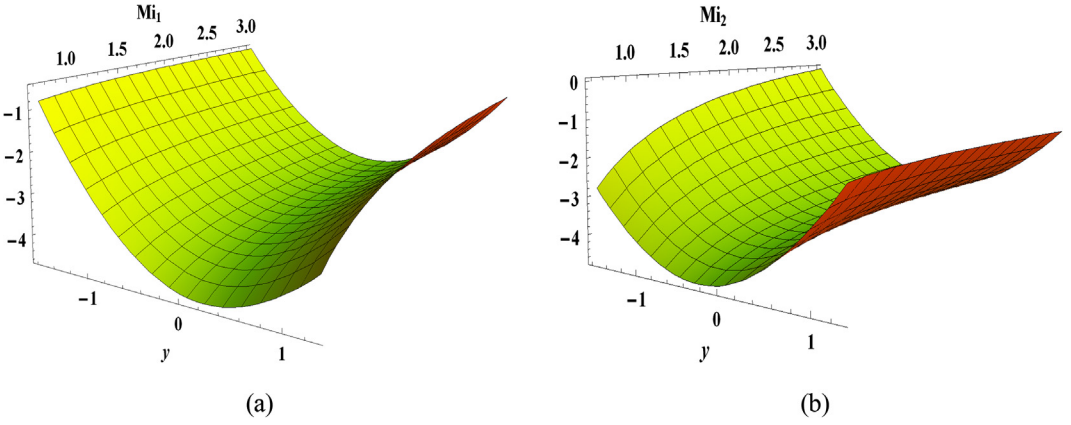

Fig. 6. Concentration variation for different mass transfer Biot-numbers when $a = 0.3$, $x = 0$, $b = 0.5$, $d = 1.2$, $Sc = 0.7$, $\eta = 1.6$, $Bi_1 = 2$, $Bi_2 = 1$, $D_f = 1$, $M = 2$, $Sr = 0.5$, $Br = 0.16$, $Sr = 0.7$ and $\beta = 1$.

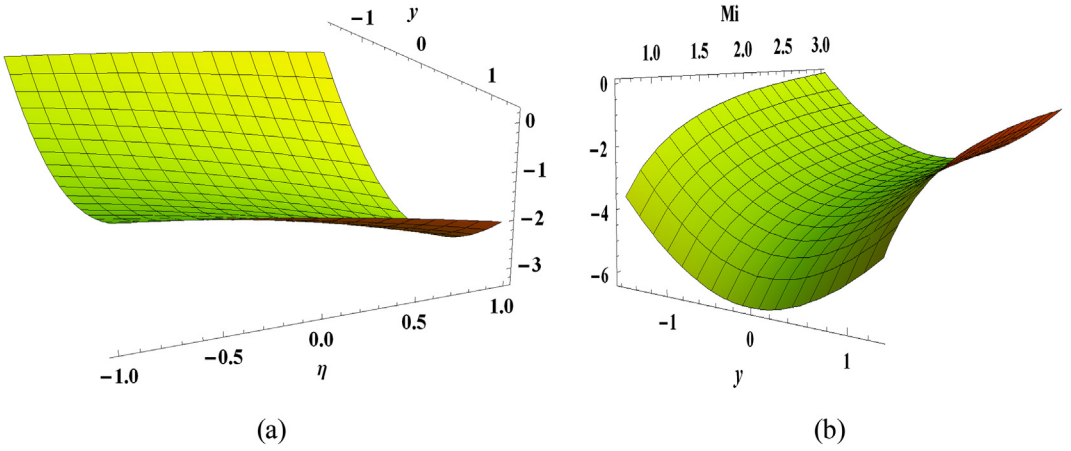

Fig. 7. Concentration variation for different flow rate and mass transfer Biot-number when $a = 0.3$, $b = 0.5$, $x = 0$, $d = 1.2$, $Sc = 0.7$, $Bi_1 = 2$, $Bi_2 = 1$, $D_f = 1$, $M = 2$, $Sr = 0.5$, $Br = 0.16$, $Sr = 0.7$ and $\beta = 1$.

(see Fig. 5). Maximum decrease is observed near the center of the channel in all the graphs. Effects of mass transfer Biot-numbers for the upper walls are shown in Fig. 6. As in the case of heat transfer Biot-number, mass transfer Biot number for one wall has no impact on transfer rate at the opposite wall. Different mass transfer Biot numbers generate a non-uniform concentration profile throughout the channel cross section. Increase in mean flow rate decreases the concentration which is very well justified physically. The dimensionless concentration field increases uniformly when upper and lower walls have similar mass transfer Biot numbers. Again the maximum change is observed for $Mi \leqslant 1$. It depicts that the concentration is higher for moving fluid than the static liquid in which the transfer only takes place through diffusion (see Fig. 7).

Conclusions

In this piece of research, phenomenon of convective temperature and concentration conditions in hydromagnetic peristaltic transport of viscous liquid is considered. Special attention is focused on the results of concentration and temperature distributions. It is visualized that the liquid temperature is enhanced with the enhancing values of Soret-Dufour parameters. The liquid temperature is reduced when the values of Biot number are larger and very weak away from the wall. It is also examined that mass transfer Biot number for one wall has no impact on transfer rate at the opposite wall. Different mass transfer Biot numbers generate a non-uniform concentration profile throughout the channel cross section. Increase in mean flow rate decreases the concentration which is very well justified physically. Comparative analysis of present results indicates that these results are in excellent agreement with the previously available ones in the qualitative sense. The results reported in Refs. [16,17] are qualitatively verified by present study.

Conflict of Interest

The authors have declared no conflict of interest.

Compliance with Ethics Requirements

This article does not contain any studies with human or animal subjects.

Appendix A. Appendix: We include the values involved in equations of solution

$$g_1 = e^{2M(h_1+h_2-y)}(A_2 + e^{2My}),$$

$$g_2 = 4e^{M(h_1+h_2-y)}A_3 - 4e^{My}A_4 + y^2A_5,$$

$$g_3 = \frac{-(1-Bi_2h_2)}{2A_1}(A_7 + Bi_1A_8),$$

$$g_4 = \frac{-(1-Bi_1h_1)}{2A_1}(A_9 + Bi_1A_{10}),$$

$$g_5 = e^{2M(h_1+h_2-y)} - 4e^{M(2h_1+h_2-y)} - 4e^{M(h_1+2h_2-y)} + e^{2My} - 4e^{M(h_1+y)} - 4e^{M(h_2+y)},$$

$$g_6 = M^2A_{12} + (2 + h_1M - h_2M)^2\beta,$$

$$g_7 = M^2A_{12} + (2 - h_1M + h_2M)^2\beta,$$

$$g_8 = M^2A_{12} + (-4 + (h_1 - h_2)^2M^2)\beta, A = \mathrm{Pr}ScSrDu,$$

$$g_9 = -((1 - Mi_2h_2)ScSrA_{15}) + 2(1 + h_1M_1)Mi_2 - (1 + h_1M_1)Mi_2ScSrA_{16},$$

$$A_1 = (-1 + A)(e^{h_1M}(-2 + h_1M - h_2M) + e^{h_2M}(2 + h_1M - h_2M))^2,$$

$$A_2 = Ec(F + h_1 - h_2)^2M^2\mathrm{Pr},$$

$$A_3 = (e^{h_1M} + e^{h_2M})Ec(F + h_1 - h_2)^2M^2\mathrm{Pr},$$

$$A_4 = (e^{h_1M} + e^{h_2M})Ec(F + h_1 - h_2)^2M^3\mathrm{Pr},$$

$$A_5 = e^{2h_2M}(Ec(F + h_1 - h_2)^2M^4\mathrm{Pr} + (2 + h_1M - h_2M)^2\beta) + 2e^{2h_1M}(Ec(F + h_1 - h_2)^2M^4\mathrm{Pr} + (2 - h_1M + h_2M)^2\beta) + 2e^{(h_1+h_2)M}(Ec(F + h_1 - h_2)^2M^4\mathrm{Pr} + (-4 + (h_1 - h_2)^2M^2)\beta),$$

$$A_6 = Bi_1 + Bi_2 + Bi_1Bi_2h_1 - Bi_1Bi_2h_2,$$

$$A_7 = 2e^{2h_2M}(Ec(F + h_1 - h_2)^2M^3(1 + h_1M)\mathrm{Pr} + h_1(2 + h_1M - h_2M)^2\beta) + 2e^{2h_1M}(Ec(F + h_1 - h_2)^2M^3(-1 + h_1M)\mathrm{Pr} + h_1(2 - h_1M + h_2M)^2\beta) + 4e^{(h_1+h_2)M}h_1(Ec(F + h_1 - h_2)^2M^4\mathrm{Pr} + (-4 + (h_1 - h_2)^2M^2)\beta),$$

$$A_8 = e^{2h_2M}(Ec(F + h_1 - h_2)^2M^2(-3 + h_1^2M^2)\mathrm{Pr} + h_1^2(2 + h_1M - h_2M)^2\beta) + e^{2h_1M}(Ec(F + h_1 - h_2)^2M^2(-3 + h_1^2M^2)\mathrm{Pr} + h_1^2(2 - h_1M + h_2M)^2\beta) + 2e^{(h_1+h_2)M}(Ec(F + h_1 - h_2)^2M^2 + h_1^2(-4 + (h_1 - h_2)^2M^2)\beta),$$

$$A_9 = e^{2h_1M}(Ec(F + h_1 - h_2)^2M^2(1 + h_2M)\mathrm{Pr} + h_2(2 + h_1M - h_2M)^2\beta) + 2e^{2h_2M}(Ec(F + h_1 - h_2)^2M^3(-1 + h_1M)\mathrm{Pr} + h_2(2 - h_1M + h_2M)^2\beta),$$

$$A_{10} = e^{2h_1M}(Ec(F + h_1 - h_2)^2M^4(-3 + h_1^2M^2)\mathrm{Pr} + h_2^2(2 + h_1M - h_2M)^2\beta),$$

$$A_{11} = Mi_1 + Mi_2 + (h_1 - h_2)Mi_1Mi_2,$$

$$A_{12} = Ec(F + h_1 - h_2)^2M^2\mathrm{Pr},$$

$$A_{13} = Ec(F + h_1 - h_2)^2M^3(-3Mi_1 + M(2 + h_1M(2 + h_1Mi_1)))\mathrm{Pr} + h_1(2 + h_1M - h_2M)^2(2 + h_1Mi_1)\beta,$$

$$A_{14} = Ec(F + h_1 - h_2)^2M^2(-3Mi_1 + M(-2 + h_1M(2 + h_1Mi_1)))\mathrm{Pr} + h_1(2 - h_1M + h_2M)^2(2 + h_1Mi_1)\beta,$$

$$A_{15} = Ec(F + h_1 - h_2)^2M^2(-4Mi_1 + h_1M^2(2 + h_1Mi_1))\mathrm{Pr} + h_1(-4 + (h_1 - h_2)^2M^2)(2 + h_1Mi_1)\beta,$$

$$A_{16} = e^{2h_2M}(MA_{12}(-1 + h_2M) + h_2(2 + h_1M - h_2M)^2\beta)(e^{2h_2M} + e^{2h_1M} + M^2 2e^{(h_1+h_2)M}h_2).$$

References

[1] Latham, TW. Fluid motion in a peristaltic pump. M S Thesis, Massachusetts Institute of Technology, Cambridge MA 1966.
[2] Shapiro AH, Jaffrin MY, Wienberg SL. Peristaltic pumping with long wavelengths at low Reynolds number. J Fluid Mech 1969;37. 799-25.
[3] Shehzad SA, Abbasi FM, Hayat T, Alsaadi F, Mousa G. Peristalsis in a curved channel with slip condition and radial magnetic field. Int J Heat Mass Transf 2015;91:562–9.

[4] Mekheimer Kh S, Husseny SZA, Abd Elmaboud Y. Effects of heat transfer and space porosity on peristaltic flow in a vertical asymmetric channel. Numer Meth Partial Diff Eqn 2010;26:747–70.
[5] Shehzad SA, Abbasi FM, Hayat T, Alsaadi F. Model and comparative study for peristaltic transport of water based nanofluids. J Mol Liq 2015;209:723–8.
[6] Tripathi D. A mathematical model for swallowing of food bolus through the oesophagus under the influence of heat transfer. Int J Therm Sci 2012;51. 91-01.
[7] Mekheimer KhS, Komy SR, Abdelsalamd SI. Simultaneous effects of magnetic field and space porosity on compressible Maxwell fluid transport induced by a surface acoustic wave in a microchannel. Chin Phys B 2013;22:124702.
[8] Abd elmaboud Y. Influence of induced magnetic field on peristaltic flow in an annulus. Commun Nonlinear Sci Numer Simulat 2012;17:685–98.
[9] Mekheimer KhS, Abd Elmaboud Y, Abdellateef AI. Particulate suspension flow induced by sinusoidal peristaltic waves through eccentric cylinders: thread annular. Int J Biomath 2013;6:1350026.
[10] Eldabe NT, Kamel KA, Abd-Allah GM, Ramadan SF. Heat absorption and chemical reaction effects on peristaltic motion of micropolar fluid through a porous medium in the presence of magnetic field. Afr J Math Comput Sci Res 2013;6. 94-01.
[11] Tripathi D. Study of transient peristaltic heat flow through a finite porous channel. Math Comput Model 2013;57:1270–83.
[12] Abbasi FM, Hayat T, Alsaedi A, Ahmed B. Soret and Dufour effects on peristaltic transport of MHD fluid with variable viscosity. Appl Math Inf Sci 2014;8:211–9.
[13] Abbasi FM, Alsaedi A, Alsaadi FE, Hayat T. Hall and Ohmic heating effects on the peristaltic transport of Carreau-Yasuda fluid in an asymmetric channel. Z Naturforsch A 2014;69:43–51.
[14] Abbasi FM, Hayat T, Ahmad B. Numerical analysis for peristalsis of Carreau-Yasuda nanofluid in an asymmetric channel with slip and Joule heating effects. J Eng Thermophys 2016;25:548–62.
[15] Hayat T, Ahmed B, Abbasi FM, Ahmad B. Mixed convective peristaltic flow of carbon nanotubes submerged in water using different thermal conductivity models. Comput Meth Prog Biomed 2016;135:141–50.
[16] Hayat T, Yasmin H, Alhuthali MS, Kutbi MA. Peristaltic flow of a non-Newtonian fluid in an asymmetric channel with convective boundary conditions. J Mech 2013;29. 599-07.
[17] Abbasi FM, Ahmed B, Hayat T. Peristaltic flow in an asymmetric channel with convective boundary conditions and Joule heating. J Cent South Uni 2014;21:1411–6.